Received: 12 February 2022 | Revised: 7 May 2022 | Accepted: 10 June 2022

DOI: 10.1002/poc.4401

RESEARCH ARTICLE

Journal of Physical Organic Chemistry WILEY

Synthesis, optical nonlinear properties, and all-optical switching of curcumin analogues

Ayman G. Faisal[1] | **Qusay M. A. Hassan**[2] | **Tahseen A. Alsalim**[3] | **H. A. Sultan**[2] | **Fadhil S. Kamounah**[4] | **C. A. Emshary**[2]

[1]Department of Applied Marine Sciences, College of Marine Sciences, University of Basrah, Basrah, Iraq

[2]Department of Physics, College of Education for Pure Sciences, University of Basrah, Basrah, Iraq

[3]Department of Chemistry, College of Education for Pure Sciences, University of Basrah, Basrah, Iraq

[4]Department of Chemistry, University of Copenhagen, Copenhagen, Denmark

Correspondence
Qusay M. A. Hassan, Department of Physics, College of Education for Pure Sciences, University of Basrah, Basrah 61001, Iraq.
Email: qusayali64@yahoo.co.in

Abstract

The curcumin analogues (Cur-MeS and Cur-MeO) are synthesized using the 3-chloroacetyl acetone and aromatic aldehydes reaction. Both compounds are characterized using FTIR, LC-MS, ^{1}H NMR, and ^{13}C NMR spectroscopies. The geometric optimization and thermodynamic properties of the two compounds are carried out theoretically using DFT. The highest HOMO, lowest LUMO, and Mullikan atom charges of the two compounds are calculated using the B3LYP and CAM-B3LYP methods which are hybrid functionals with a 6-311+G(2d,p) as the basis set. The nonlinear optical (NLO) properties of both compounds are studied using the spatial self-phase modulation (SSPM) through the diffraction ring patterns (DRPs) and the *Z*-scan techniques, using a continuous wave (cw) low power 473 nm laser beam. The index of nonlinear refraction (INR) of both compounds is calculated by the two techniques. The all-optical switching property of both samples is tested using two visible cw laser beams.

KEYWORDS

all-optical switching, curcumin analogues, DFT, *Z*-scan

1 | INTRODUCTION

During the last three decades, there has been great needs for materials with high optical nonlinearities and fast response times which can be used with low power laser beams,[1–10] in variety of applications such as optical switching,[11,12] imaging processing,[13] data storage,[14–17] phase conjugation,[18] and optical limiting.[19–25]

When a laser beam with fundamental, TEM_{00}, transverse mode and continuous wave (cw) traverses a material, an intensity-dependent refraction index can be observed in the medium. The refraction index change of a medium can be determined via the spatial self-phase modulation (SSPM) due to the intensity-dependent refractive index that has been observed since 1967 in so many materials in the shape of diffraction ring patterns (DRPs) and the *Z*-scan techniques. Owing to the first technique, the total refractive index change and the index of nonlinear refraction (INR) of the medium can be determined using the total number of rings. The *Z*-scan is an effective and simple technique that was pioneered by Sheik-Bahae et al.,[26] usually used to determine the INR and absorption nonlinear coefficient (ANC), the sign of the INR, real and imaginary parts of the nonlinear susceptibility, and so on. In the *Z*-scan, self-focusing (SF) or self-defocusing (SDF) leads to a valley succeeded by a peak or a peak succeeded by a valley respectively in the relations between the normalized transmittance of the laser beam versus the sample cell position *Z*-scan.

The curcumin compounds and their isomers called diferuloylmethane are extracted from turmeric (*Curcuma longa* Linn).[27–29] Because it is not harmful, diferuloylmethane is used to treat wide variety of human diseases. With its unique properties, they can be used in biological and pharmacological functions,[30] including antioxidant,[31–34] anti-inflammatory,[35] and anti-cancer,[36–42] as well as natural yellow food pigment (commercial code E100).[43] Curcumin is an unsaturated hydrophobic structure of β-diketone that exhibits keto-enol form in aqueous solutions and organic solvents like ethanol.[44,45] FTIR spectroscopy has been employed to determine the change of the keto-enol equilibrium towards the enol form in tautomers,[46] fluorescence,[47–49] and ^{1}H NMR.[50] These techniques have revealed that the enol form is the main tautomer as a crystal structure, which has been confirmed by several computational studies.[51–58] Our continuous search for curcumin and its compounds is due to the functional value of these biomolecules in pharmaceutical, medicinal, biophysical, and bioorganic chemistry with pronounced physiological activities.[33,36,59] Curcumin was studied in a number of scientific applications.[60–62] We have been engaged in the period 2018–2020 in the study and improve the nonlinear properties of bisdemethoxycurcumin,[63] curcumin, dimethoxycurcumin, chlorocurcumin,[64] alpha-methyl curcumin: PMMA film using gamma radiation,[65] and two dihydropyridones derived from curcumin.[66]

The main objective of the current study is to find new materials, such as curcumin compounds, as far as we know, its nonlinear optical (NLO) properties have not been studied previously, that has high NLO properties, for the purpose of using it in photonic applications such as the optical limiter, optical switch, and others. To achieve this purpose, two curcumin analogues, Cur-MeS and Cur-MeO, were synthesized via the reaction of the 3-chloroacetyl acetone and appropriate aldehydes. The two compounds were characterized via FTIR, mass, ^{1}H NMR, and ^{13}C NMR spectroscopies. The electronic structural and thermodynamic properties of the two compounds were theoretically investigated. The INR of the prepared two compounds was determined via the SSPM and *Z*-scan techniques using cw, single TEM_{00} mode, low power, and visible 473 nm laser beam. The DRPs dependent on the input power, on the type of the laser beam wavefront together with their temporal behavior, were studied. The all-optical switching property for these two compounds was tested and proved to occur using laser beams of wavelengths 473 and 532 nm.

2 | EXPERIMENTAL

2.1 | Instrumentation

The starting reagents, materials, and solvents were supplied by Fluka, Merck, Sigma, and Fischer. IR spectra were recorded using Shimadzu FTIR (affinity-1) in the range of 4000–400 cm^{-1}. ^{1}H NMR and ^{13}C NMR spectra were determined using Brucker 500 spectrometer and tetramethylsilane (TMS) as an internal standard and DMSO-d_6 as solvents. Chemical shifts (δ) were evaluated in ppm and coupling constants in Hz. Mass spectra were scanned using the EI technique at 70 eV on Agilent 5975 C spectrometer and electrospray ionization (ESI) using (SynaptG2 MS water) at 3–5 eV. Electron spectra were measured using a T80+ PG instrument in ethanol using a quartz (0.1 cm) cell.

2.2 | The general method for the synthesis of curcuminoids (Cur-MeS and Cur-MeO)

In the reaction flask, chloroacetyl acetone (6 g, 0.046 mol) and boric oxide (3.09 g, 0.0438 mol) were mixed in dry dimethylacetamide (50 ml) for 1 h. To this content, the necessary aldehyde (0.39 mol) and trimethyl borate 9.69 g (0.93 mol) dissolved in dimethylacetamide (75 ml) were added in a water bath (80°C). The reaction mixture was stirred for 10 min; then, a solution of *n*-butylamine (1.5 ml, 0.018 mol) in DMA was added dropwise over 1 h, and the mixture was stirred for another 3 h. After leaving the mixture overnight, 120 ml of 5% glacial acetic acid was added and the mixture was stirred for 1 h at 80°C. After the completion of the reaction, cooling and filtration of the mixture were performed.

2.2.1 | [(1*E*,6*E*)-4-Chloro-1,7-bis (4-(methylthio)phenyl)hepta-1,6-diene-3,5-dione] (Cur-MeS)

Isolated as orange crystals, recrystallized from ethanol, yield: 43%, M.p.: 185°C to 187°C. ^{1}H NMR (DMSO, δ ppm): 2.53 (6H, s, SCH_3), 7.32 (2H, d, $J = 5$, olefinic protons), 7.40 (4H, d, $J = 15$, Ar–H), 7.68 (4H, d, $J = 5$, Ar–H), 7.73 (2H, d, $J = 10$, olefinic protons). ^{13}C NMR (DMSO, ppm) 14.7, 110.0, 125.7, 126.1, 129.4, 131.6, 142.2, 142.5, 188.7. IR (υ, cm^{-1}): 3022, 2974, 1612, 1587, 1562, 1492, 1408, 1379, 1369, 1325, 1184, 1093, 970, 812. MS-EI (70 eV, m/z); 402 [M], 368, 339, 312, 225, 272, 242, 177 [base peak], 146, 137, 116, 110, 89, 67, 43.

2.2.2 | [(1*E*,6*E*)-4-Chloro-1,7-bis (4-methoxyphenyl)hepta-1,6-diene-3,5-dione] (Cur-MeO)

This compound was synthesized based on the procedure described elsewhere.[36]

2.3 | Theoretical calculations

The molecular properties and theoretical calculations of the synthesized compounds (Cur-MeS and Cur-MeO) were investigated via density functional theory (DFT) using the B3LYP method. The geometrical optimizations for the synthesized compounds were performed using DFT/B3LYP 6-311+G(2d,p), and DFT/CAM-B3LYP 6-311+G(2d,p) basis set was used to calculate the optimized data.

2.4 | Experimental setups

A solid-state laser device emitting 0–66 mW, cw, at 473 nm laser beam was used as the irradiation source of light in the generation of DRPs. The laser beam of radius of 1.5 mm was focused on the sample glass cells of thickness 0.1 cm using a glass double convergent lens of 50 mm focal length where the radius of the beam at the entrance of the sample cell was 19.235 μm. The DRPs due to the SSPM were observed on a semitransparent 30 × 30 cm screen, a distance 85 cm from the sample cell exit plane. The images of DRPs were recorded by a digital camera.

The *Z*-scan experiments were performed using the same setup used in obtaining DRPs with the following modifications. The sample cell was fixed on a translation stage for the sake of translation between $(-z)$ and $(+z)$ passing through the lens focal point $(z = 0)$ along the propagation direction. The laser beam transmittances were measured through an aperture of 2 mm diameter covering the power meter, that is, the closed aperture (CA) *Z*-scan. The open aperture (OA) *Z*-scan experiments were carried out by collecting the entire transmitted laser beam power via replacing of the aperture with another convergent double glass lens.

The all-optical switching experiments were conducted using two laser beams, namely, 473 and 532 nm, via the cross-passing technique horizontally.[67] Both laser beams have variable powers (0–66 and 0–50 mW, respectively) and the same properties. A 60 × 60 cm semitransparent screen was used to cast the DRPs due to the two laser beams and two positive glass lenses of focal length of 20 cm for the sake of focusing the two beams onto the sample cell.

3 | RESULTS AND DISCUSSION

3.1 | Experimental results

Curcumin analogues (Cur-MeS and Cur-MeO) were synthesized from the condensation of 3-chloroacetyl acetone with the appropriate aldehyde (Figure 1). The proposed structures have been confirmed by using spectroscopic techniques; both compounds showed satisfactory spectroscopic analyses for the proposed structures. And this section represents a description of the spectroscopic data of the synthesized compounds.

3.1.1 | IR spectra

The IR spectra of the synthesized compounds showed that the functional group bands were in the expected regions. All IR spectra showed weak bands in the ranges (3022–3011) and (2974–2895) cm^{-1}, which are attributed to aromatic C—H and aliphatic C—H, respectively. Strong bands were obtained for the stretching vibration of the C═O, C═C, and C—O groups at (1615–1612), (1592–1587), and (1255) cm^{-1}, respectively, for Cur-MeO. Figure S1 shows the IR spectrum of Cur-MeS.

3.1.2 | Mass spectrum of compound Cur-MeS

The mass spectrum was employed to determine the molecular ion and the base peak. The peak intensity provides information on the stability of the fragment. The mass spectrum of the synthesized Cur-MeS compound (Figure S2) showed the molecular ion (M^+) and the main direction of fragmentation that resulted from breaking the bond of the chelating group between the methylene and carbonyl group. Other fragments were obtained by cleaving the bonds at different positions and forming other bonds (Figure S3).[68]

3.1.3 | ^{1}H NMR and ^{13}C NMR spectra

The ^{1}H NMR spectral data of curcumin analogues synthesized in DMSO-d_6 at 25°C confirm the proposed structure. The spectrum of the compound Cur-MeO displayed a singlet signal at δ 3.83 ppm, which is attributed to the protons of the methoxy group, two doublet signals from olefinic protons at δ 6.98 ppm, δ 7.74 ppm, and two doublet signals at 7.31 and 7.65 ppm attributed to aromatic protons. Furthermore, the spectrum of the Cur-MeS compound (Figure S4a) displayed three signal groups and

aromatic and olefinic protons appearing in the same range of 7.32–7.73 ppm, while MeS proton appeared at δ 2.53 ppm.

The ^{13}C NMR spectra of both compounds exhibited carbon signals from the carbonyl group (C═O) within (180.4–188.7) ppm. Also, the spectra displayed signals within (143–110) ppm attributed to aromatic and olefinic carbon; the MeO carbon signal was obtained at 56.6 ppm, while the MeS carbon signal was obtained at 14.7 ppm (Figure S4b).

3.1.4 | Computational results

The B3LYP and CAM-B3LYP methods were used to do all theoretical computations via the 6-311+G(2d,p) basis set. Figure 2 shows the optimized structures and atomic labeling of both compounds. As a nonplanar construction, the image shows the geometrical optimization yields. B3LYP/6-311+G(2d,p) and CAM-B3LYP/6-311+G (2d,p) basis sets were also used to calculate the optimized data.

3.1.5 | Electronic properties and quantum chemical descriptors (QCDs)

Plots of the border molecular orbitals for the compounds produced demonstrate the energetic character of the chemical (Figure 3). In the structure, the LUMO was predominantly localized on the benzene ring, oxygen, and sulfur atom, and the HOMO was localized in the structure. This shows that the frontier molecular orbital is vital in hydrophobic interactions and *p–p* stacking, thus, leading to good interaction between the compounds and residue receptor chains. Small energy gaps were found for the compounds Cur-MeS and Cur-MeO. This revealed that the synthesized compounds have high reactivity and polarizability. The parameter values are listed in Tables 1 and 2.

From the mentioned facts about the importance of NLO properties in previous studies of curcumin and their analogues,[69–75] we have studied the NLO properties of curcumin analogues (Cur-MeS and Cur-MeO). The investigations of NLO characteristics on a theoretical-level DFT/B3LYP and DFT/CAM-B3LYP

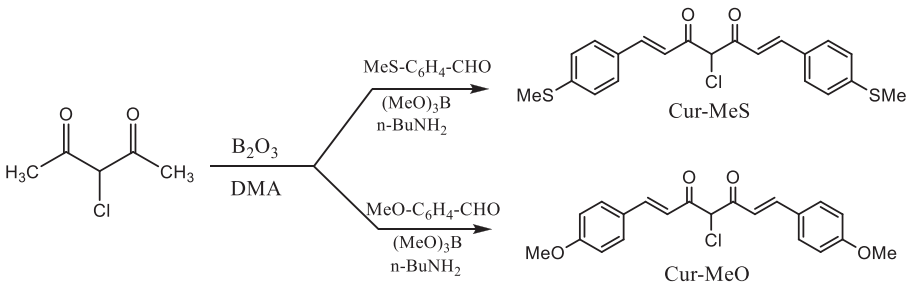

FIGURE 1 Synthetic routes of curcumin analogues

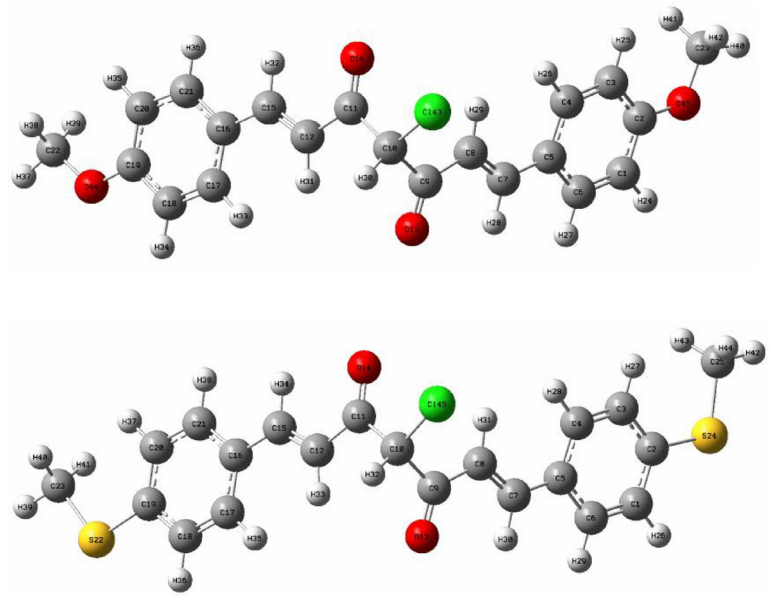

FIGURE 2 The optimized structures of synthesized compounds (Cur-MeS and Cur-MeO) within a number of atoms

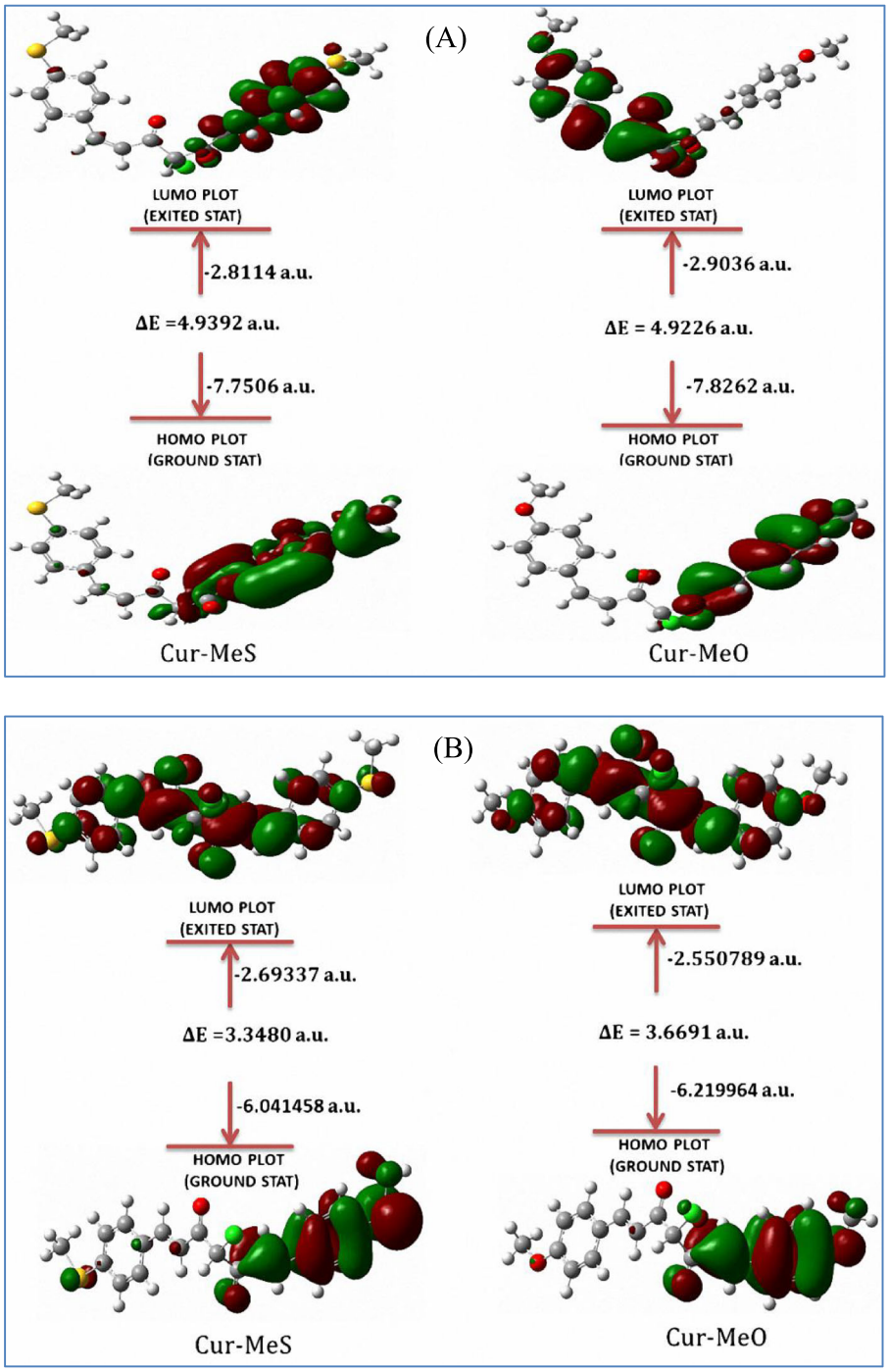

FIGURE 3 The compositions of atomic orbital of the frontier molecular orbital for the synthesized compounds Cur-MeS and Cur-MeO. (A) Using DFT/B3LY 6-311+G(2d,p). (B) Using DFT/CAM-B3LYP 6-311+G(2d,p)

methods with 6-311+G(2d,p) basis set have been used to generate several QCDs to investigate the NLO properties. Increases in E_{HOMO}, softness means (S), and optical softness (S_o) indicate that NLO qualities are growing. The NLO characteristics increase as E_{LUMO}, energy gap, ionization potential IE, and hardness decreases. The E_{HOMO}, S, and S_o values of the synthesized compounds, Cur-MeS and Cur-MeO, were greater, whereas the E_{LUMO}, E_{gap}, and ionization potential IE were lower, indicating that they have better NLO characteristics.[76]

Table 2 shows an overview of the results. In the computational study of curcumin dye[75] within level DFT/B3LYP 631-G+(d,p). The values of HOMO energy and LUMO energy were −5.72 and −2.51 eV, respectively. A lower HOMO–LUMO energy gap (−3.21 eV). The quantitative chemical descriptors were calculated (Table 2); the results show the closeness of the values between curcumin dye and synthesized analogues (Cur-MeO and Cur-MeS). Also indicating that they have NLO characteristics like curcumin dye.

CAM-B3LYP was used to calculate the ground-state and excited-state geometries utilizing 6-311+G(2d,p) basis sets. The smaller HOMO–LUMO energy gap (4.504 and 4.336 eV) for Cur-MeS and Cur-MeO, respectively, shows the molecule's chemical activity and explains how charge–transfer interaction occurs. QCDs were determined (Table 2). They exhibit NLO features, according to the results.

3.1.6 | Mulliken population analysis

Mulliken atomic charge calculations are important when applying quantum chemical calculations to molecular systems because atomic charges affect the features such as dipole moment and molecular polarization. Figure 4 represents the atomic charges of the compounds (Cur-MeS and Cur-MeO) that were produced using the Mulliken population. All hydrogen atoms were shown to possess positive charges. Furthermore, the Mulliken atomic charges confirmed that the C2 and C19 atoms in the benzene ring (two sides) have a positive charge due to the presence of electronegative sulfur atom (S), while the C2 and C10 atoms in the compound Cur-MeO have a moderate positive charge due to the presence of electronegative oxygen, resulting in having more reaction sites in these atoms. The other atoms (O13, O14, S22, and S24) are all negative, as one would anticipate.

3.1.7 | NMR analysis

Calculations of ^{13}C NMR chemical shifts were recorded to compare experimental and theoretical NMR data that can be helpful to determine appropriate assignments and understand the relationship between chemical shifts and molecular structure. The experimental data were compared with estimated values to determine the relationship between the theoretical and experimental values of NMR chemical shift constants.

TABLE 1 The calculated thermodynamic parameters for the compounds (Cur-MeS and Cur-MeO) using DFT/B3LYP /6-311+G(2d,p) and CAM-B3LYP/6-311+G (2d,p)

	CAM-B3LYP/6-311+G(2d,p)		B3LYB/6-311+G(2d,p)	
Parameters	**Cur-MeS**	**Cur-MeO**	**Cur-MeS**	**Cur-MeO**
Zero-point vibrational energy (kcal/mol)	0.347819	0.355271	0.351896	0.359613
Entropy (S) (cal/mol/K)	192.744	182.337	186.984	176.823
Dipole moment (μ) (Debye)	2.6044	3.6826	3.918367	4.2744
Electronic energy (EE) (Hartree)	-2218.4935	-1572.5041	-1759.4265	-1113.4635
Specific heat (C_v) (cal/mol/K)	94.803	90.755	92.924	88.745

TABLE 2 Some QCDs of NLO properties calculated for Cur-MeS and Cur-MeO

Calculation methods	**Compound**	E_{HOMO} (eV)	E_{LUMO} (eV)	Ionization potential (IE) − E_{HOMO} (eV)	Electron affinity (EA) − E_{LUMO} (eV)	E_{gap} (E_{LUMO} − E_{HOMO}) (eV)
B3LYP	Cur-MeS	−6.041	−2.693	6.041	2.693	3.348
	Cur-MeO	−6.219	−2.550	6.219	2.550	3.669
CAM-B3LYP	Cur	−5.72	−2.51	5.72	2.51	3.21
	Cur-MeS	−7.407	−2.904	7.407	2.904	4.504
	Cur-MeO	−7.228	−2.892	7.228	2.892	4.336

Calculation Methods	**Compound**	**Hardness η (eV) ($\eta = (IE - EA)/2$)**	**Softness S (eV^{-1}) ($S = 1/\eta$)**	**Optical softness S_o (eV^{-1}) ($S_o = S/2$)**	**Electron delocalization χ (eV) ($\chi = (IE + EA)/2$)**	**Chemical potential CP (eV) ($CP = -\chi$)**
B3LYP	Cur-MeS	1.674	0.597	0.298	4.367	−4.367
	Cur-MeO	1.834	0.545	0.272	4.384	−4.384
CAM-B3LYP	Cur	1.605	0.623	0.311	4.115	−4.115
	Cur-MeS	2.251	0.444	0.222	5.155	−5.155
	Cur-MeO	2.168	0.461	0.2305	5.06	−5.06

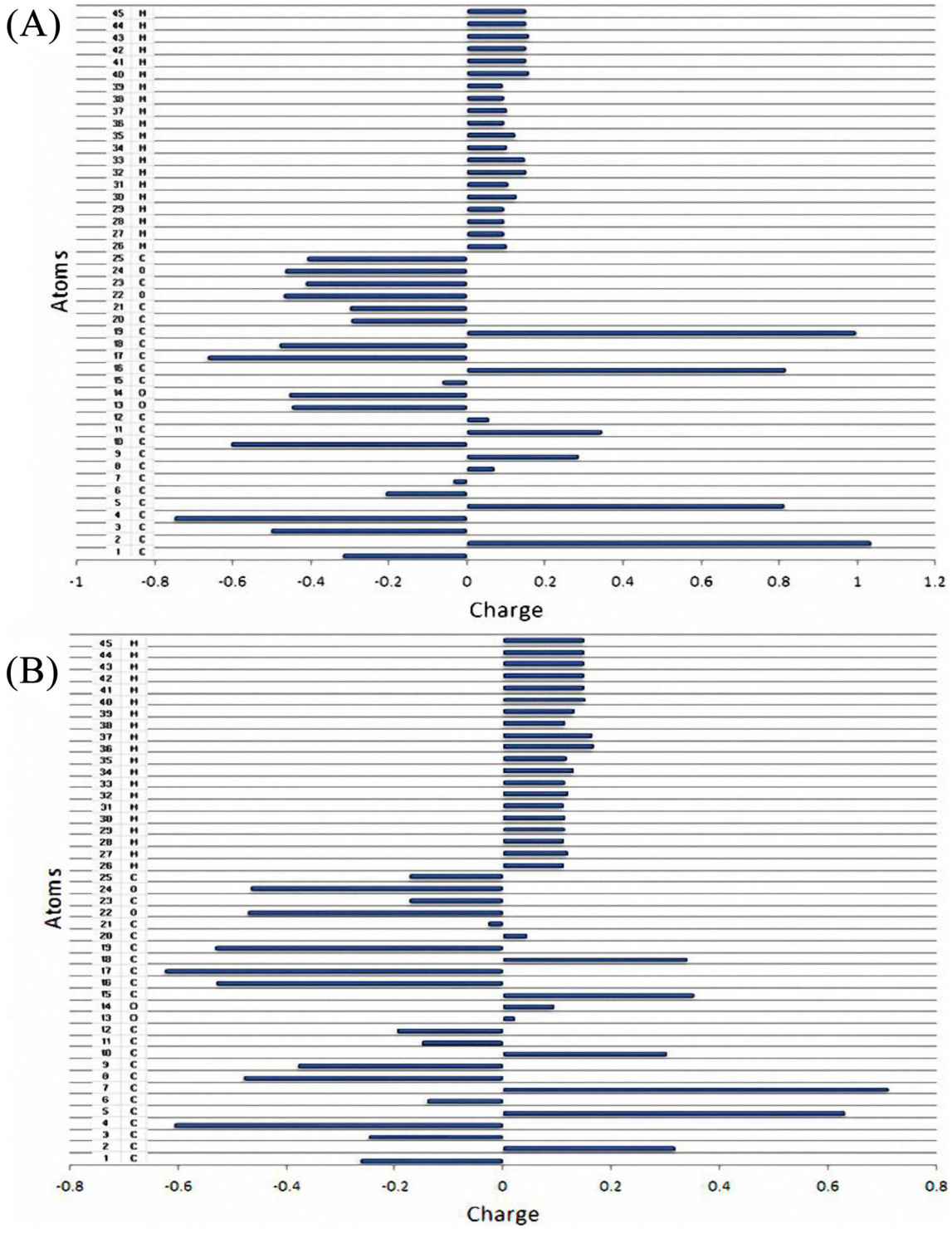

FIGURE 4 The atomic charge distribution according to Mulliken (A) of Cur-MeS compound and (B) of Cur-MeO compound

The ^{13}C NMR chemical shifts for all carbon atoms in the optimal structures of the compounds were estimated using the B3LYP method with the 6-311+G(2d,p) basis set. To quantify the ^{13}C NMR chemical shifts, each pair of carbon atoms at the same position in the molecule was considered equivalent, and the average of their chemical shifts was determined. The statistical characteristics of the calculated ^{13}C NMR chemical shifts and the experimental evidence of the compounds (Cur-MeS and Cur-MeO) are shown in Figure 5. As can be seen, the results are in reasonable agreement with the experimental values.

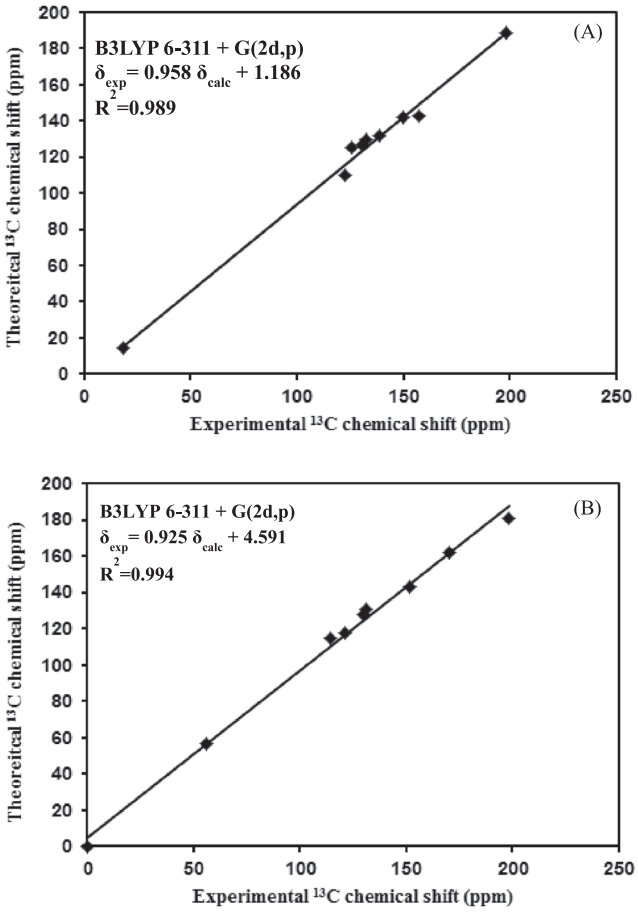

FIGURE 5 Experimental values versus theoretical ^{13}C NMR chemical shifts of (A) Cur-MeS compound and (B) Cur-MeO compound

3.1.8 | UV-visible spectroscopy

The absorbance (A) spectra of the Cur-MeS and Cur-MeO compounds solutions in the UV-visible range were obtained using a UV-visible spectrophotometric device-type T80 PG instrument at room temperature. The result of their absorbance spectra is shown in Figure 6.

The linear coefficient of absorption, α_i, for both samples are obtained at 473 and 532 nm using the absorbances (A_i) from Figure 6 and the relation[77]

$$\alpha_i = 2.303\frac{A_i}{d}. \quad (1)$$

d is the sample cell thickness. For $A_{\text{Cur-MeS}}$ and $A_{\text{Cur-MeO}}$ at 473 nm of 0.739 and 0.393, respectively, and at 532 nm of 0.032 and 0.002, respectively, $d = 0.1$ cm, so that $\alpha_{\text{Cur-MeS}}$ and $\alpha_{\text{Cur-MeO}}$ equal to 17.02 and 9.05 cm^{-1} at 473 nm, respectively, and 0.736 and 0.046 cm^{-1} at 532 nm, respectively.

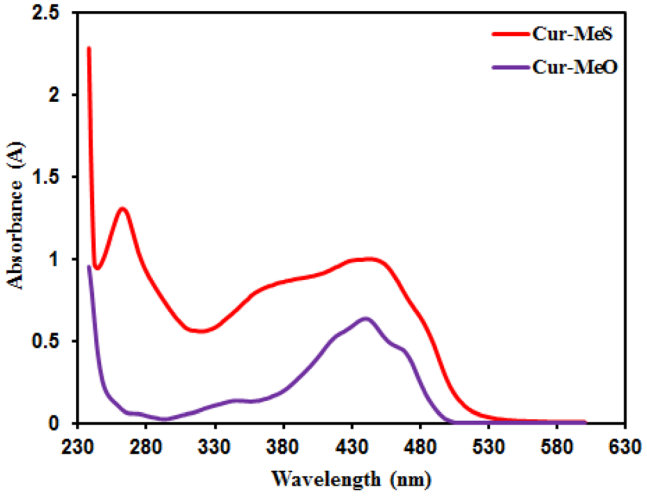

FIGURE 6 Absorbances (A) spectra of Cur-MeS and Cur-MeO compounds in the UV-visible range at room temperature

3.2 | DRPs

Figures 7 and 8 show typical far-field DRPs of the cw laser beam of wavelength 473 nm, as the input power was increased slowly, for both compounds, namely, Cur-MeS and Cur-MeO respectively, where it can be seen the increase of the areas of patterns and the number of rings in each pattern with the increased input power. Severe asymmetries occur due to the increased input power; almost the top half of each and every pattern disappear as a result of the vertical thermal convection current which seems to exceed the horizontal thermal conduction current. The vertical thermal current of convection acts on the replacement of the top hot layer by a cold one which smooth's the change in the upper part refraction index so that the phase of laser beam change severely reduced. In every pattern, the most intense rings were the outer rings compared with the inner ones, an indication of the SDF of the laser beam. The ring pattern type appears to depend on the laser beam wavefront type, namely, the interaction of nonlinear medium with laser beam depends on the type of the beam wavefronts; see Figure 9A,B for Cur-MeS and Figure 9C,D for the Cur-MeO, respectively. The ring pattern temporal behaviors are shown in Figures 10 and 11 for Cur-MeS and Cur-MeO, respectively, that is, ring number, each pattern area, and the asymmetries developed as the time lapse.

In the all-optical experiments, the exciting, or the controlling (473 nm) laser beam, and the controlled (532 nm) laser beam were set at the same height with an angle of 35° between them so that they crossed each other in the entrance of each sample as they propagate. When the controlling beam intensity, 473 nm, was 0 mW, no DRPs appear due to the controlled, 532 nm beam, that is, full spot appears. Because the absorption

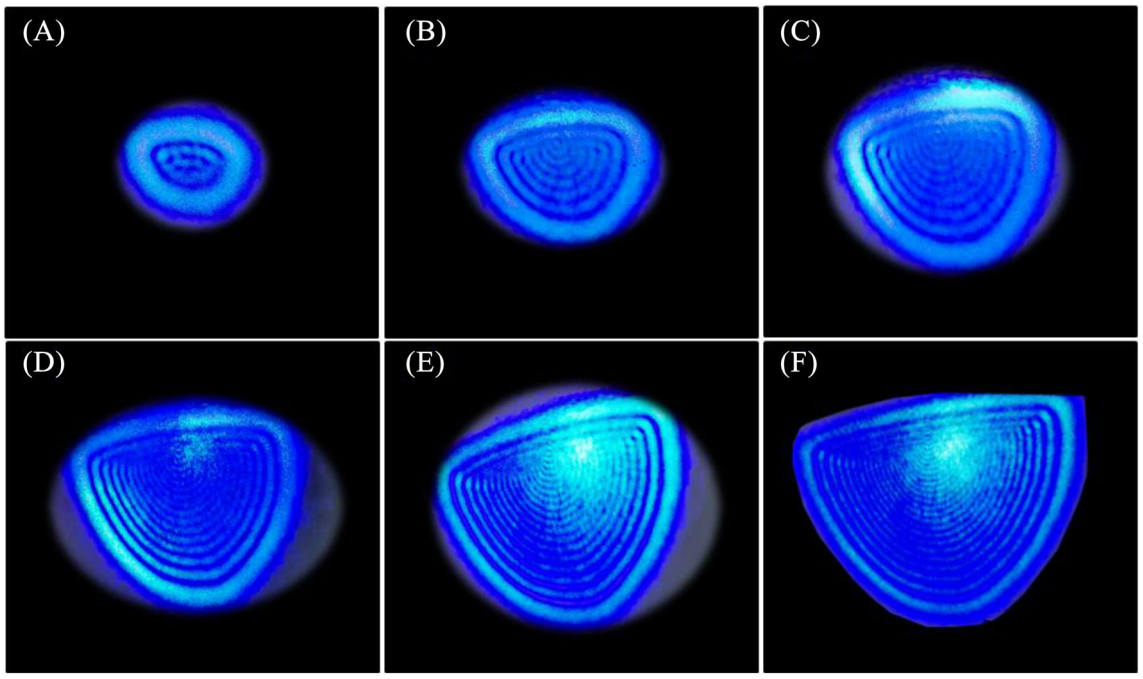

FIGURE 7 Series of far-field DRPs versus input power (mW) in Cur-MeS: (A) 13, (B) 20, (C) 30, (D) 44, (E) 52, and (F) 64

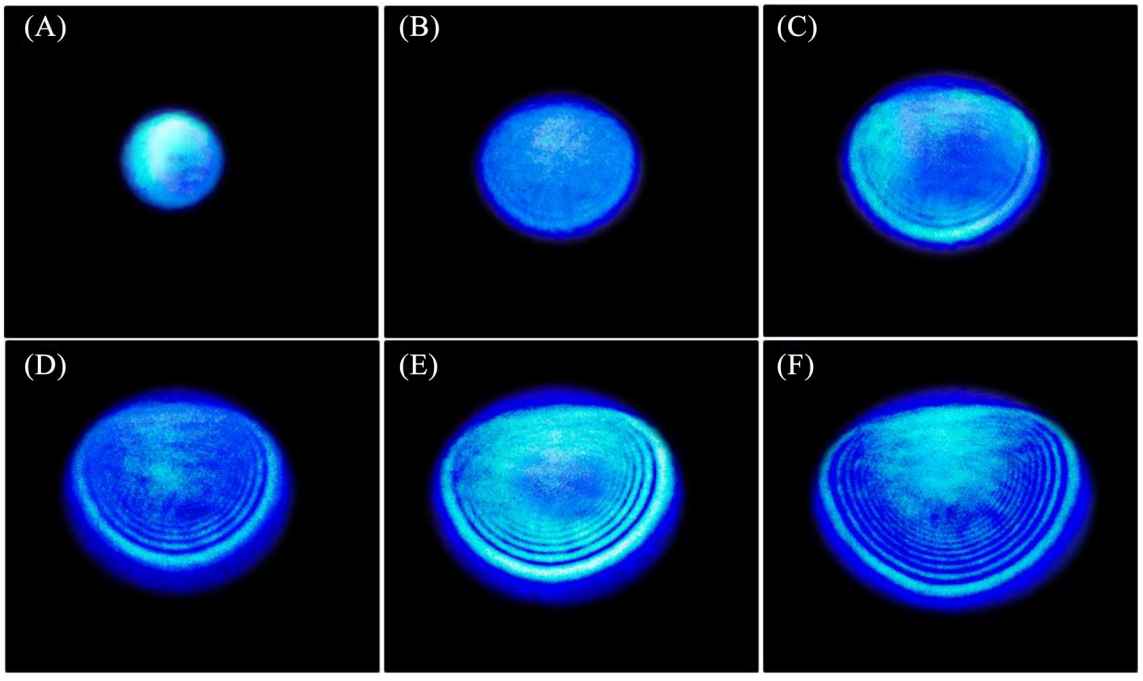

FIGURE 8 Series of far-field DRP patterns versus input power (mW) in Cur-MeO: (A) 13, (B) 20, (C) 30, (D) 44, (E) 52, and (F) 64

coefficients of the Cur-MeS and Cur-MeO at $\lambda = 473$ nm are 17.02 and 9.05 cm^{-1}, respectively, the amount of absorbed energy by the two samples is high, that is, it is possible to produce DRPs as show in Figures 7 and 8 even at low input power. In other case, for Cur-MeS and Cur-MeO, the absorption coefficients at $\lambda = 532$ nm are 0.736 and 0.046 cm^{-1}, respectively, so that minimum energy absorbed by the two samples and no DRPs appeared in the two samples even at high input power, as shown in Figures 10A and 11A for $\lambda = 532$ nm alone. When the laser beam $\lambda = 473$ nm used and even for moderate input power DRPs appeared as shown in Figures 10C and 11C which enhances DRPs due to the wavelength 532 nm as shown in Figures 10B and 11B. As the 473 nm beam

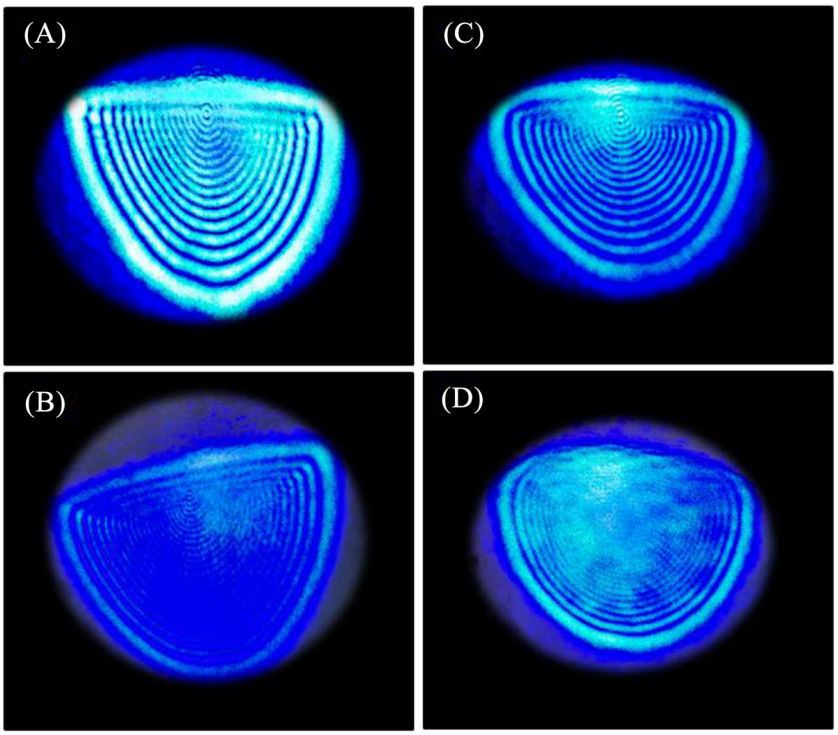

FIGURE 9 Dependence of the DRPs on the wave front of laser beam type (A) convergent and (B) divergent in the Cur-MeS and (C) convergent and (D) divergent in the Cur-MeO at input power of 64 mW

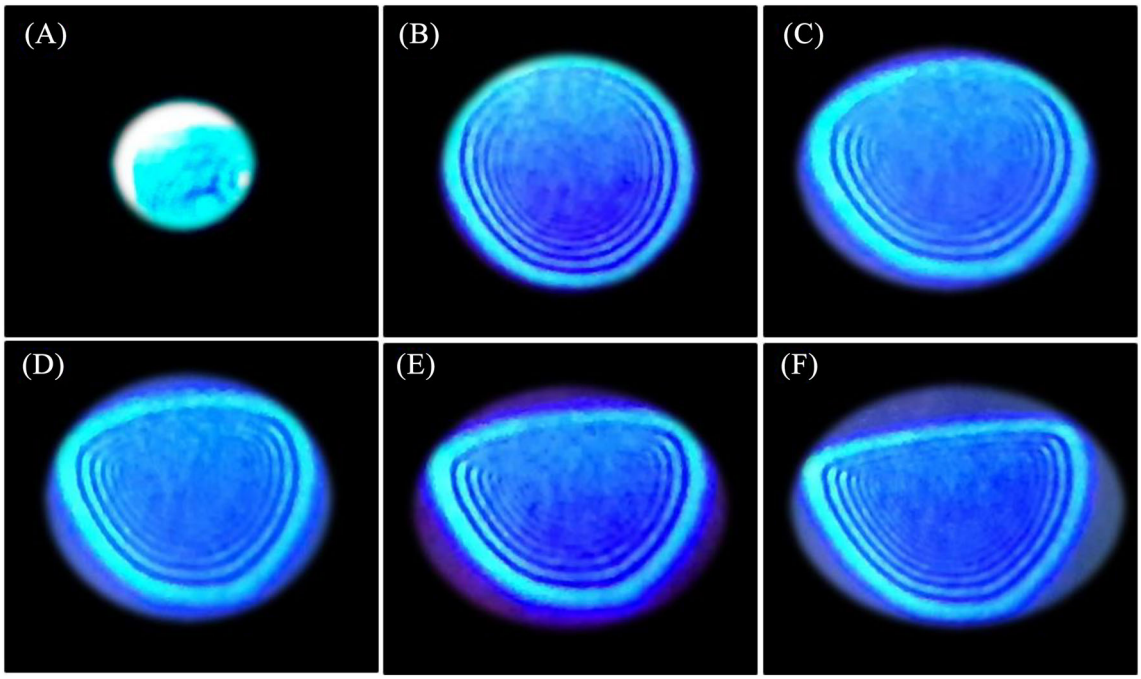

FIGURE 10 Time series in a chosen DRP at different times (ms): (A) 0, (B) 150, (C) 300, (D) 500, (E) 700, and (F) 1000 at power input 64 mW in Cur-MeS

power increased, blue rings appear together with green ones. The number of rings of the blue light increased with the increase of its intensity together with the green ones, while increasing the green input power increases the green diffraction ring intensity only. This is due to the crosstalk effect between the controlling and controlled beams which produce ring patterns due to the spatial cross-phase modulation (SXPM).[78] Figure 12 D1 (a) is the result of the irradiation with 532 nm laser beam only while Figure 12 D1 (b + c) shows diffraction rings at the 532 nm in the existence of the 473 nm beam where it can be seen that the resulting of green rings although

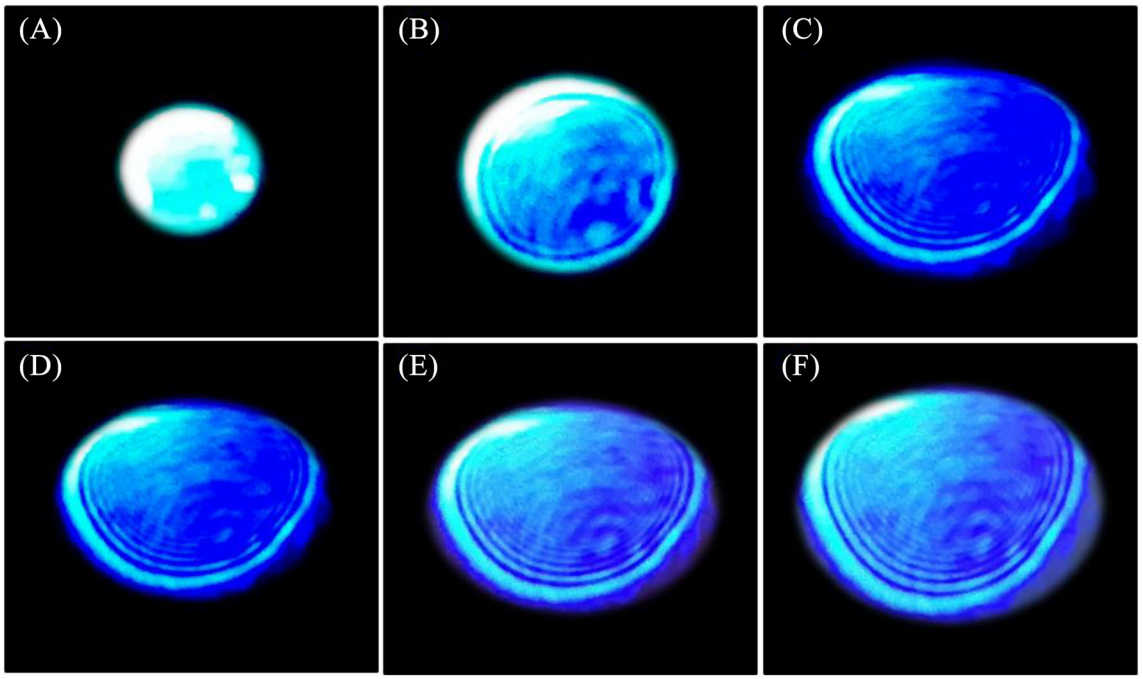

FIGURE 11 Time series in a chosen DRP at different times (ms): (A) 0, (B) 150, (C) 300, (D) 500, (E) 700, and (F) 1000 at power input 64 mW in Cur-MeO

the absorption coefficient of Cur-MeS is very low, at 532 nm. Figure 12 D2 (a + b + c) shows the effect of the beam 473 nm on blue diffraction rings, it affect the number of rings, the area of diffraction rings and the asymmetries. Figure 12 D3 (a + b + c) shows the effect of 473 nm beam power on green DRP number, the area of each pattern, and the symmetries. Figure 12 D4 (a + b +- c) shows the effect of the laser wavelength 532 nm power on the intensity of the green pattern only. All this occurs in the Cur-MeS only. The same behavior can be seen for the case of the compound Cur-MeO, that is, Figure 13.

3.3 | Calculations of the nonlinear refraction index based on

3.3.1 | Diffraction ring patterns

It can be seen from Figures 7 and 8 that the ring number in every pattern depends directly on the power input irradiation on the samples. For a single ring in a pattern to result, the refractive index of medium change should lead to a change of the laser beam phase by 2π radians. For N rings, the total change of phase, $\Delta\varphi$, the laser beam suffers due to the passage through the nonlinear medium, which is written as follows[79]:

$$\Delta\varphi = 2\pi N. \tag{2}$$

Once more, $\Delta\varphi$ can be written in terms of wave vector of laser beam ($k = \frac{2\pi}{\lambda}$) and the sample cell thickness, d, as follows:

$$\Delta\varphi = k\Delta, \tag{3}$$

$$\Delta\varphi = k\Delta n d.$$

Δ is the optical path length, and Δn is the total change in the medium refractive index, so that

$$\Delta n = \frac{N\lambda}{d}. \tag{4}$$

And INR, n_2, can be calculated using the following equation:

$$n_2 = \frac{\Delta n}{I}. \tag{5}$$

I is the laser beam intensity where

$$I = \frac{2P}{\pi\omega^2}. \tag{6}$$

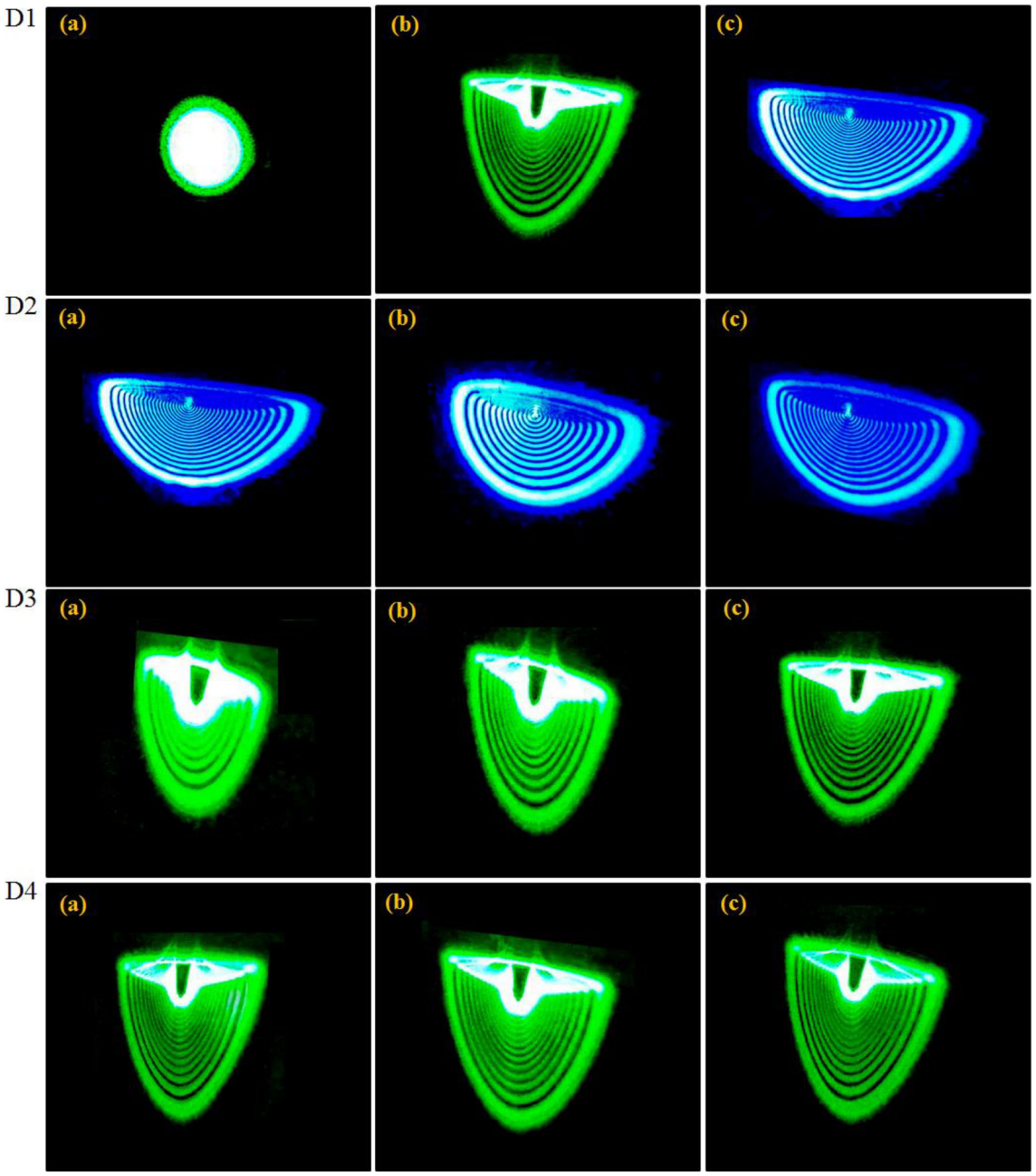

FIGURE 12 D1 (a) Single solid spot with no diffraction rings appeared in the presence of the 532 nm beam only, because the absorption coefficient in Cur-MeS is very low, D1 (b) green patterns appear in the presence of 473 nm, and D1 (c) the blue rings due to the 473 nm beam. D2 (a + b + c) shows the 473 nm beam power effect on the blue rings, D3 (a + b + c) shows the effect of the 473 nm beam on the green ring pattern number and area due to the effect of the 473 nm, and D4 (a + b + c) shows the effect of the 532 nm beam on the green intensity only. All these results are in the Cur-MeS.

P is the total power input, and ω is the laser beam radius at the sample cell entrance so that for $P = 64\,\text{mW}$, $I = 11{,}018\,\text{W/cm}^2$, $\omega = 19.235\,\mu\text{m}$, $N_{\text{Cur-MeS}}$ and $N_{\text{Cur-Meo}}$ equal to 20 and 14, respectively, $d = 0.1\,\text{cm}$, $\lambda = 473\,\text{nm}$, $\Delta n_{\text{Cur-MeS}} = 9.46 \times 10^{-3}$, $\Delta n_{\text{Cur-Meo}} = 6.62 \times 10^{-3}$, $n_{2(\text{Cur-MeS})} = 8.58 \times 10^{-7}\,\text{cm}^2/\text{W}$, and $n_{2(\text{Cur-MeO})} = 6.01 \times 10^{-7}\,\text{cm}^2/\text{W}$.

3.3.2 | *Z*-scan

We obtained the results shown in Figure 14A,B when the CA and OA *Z*-scans were carried out, respectively. From Figure 14A,B, it can be seen that both samples have negative INR and negative ANC, respectively. The negative INR indicates the occurrence of SDF, while the negative

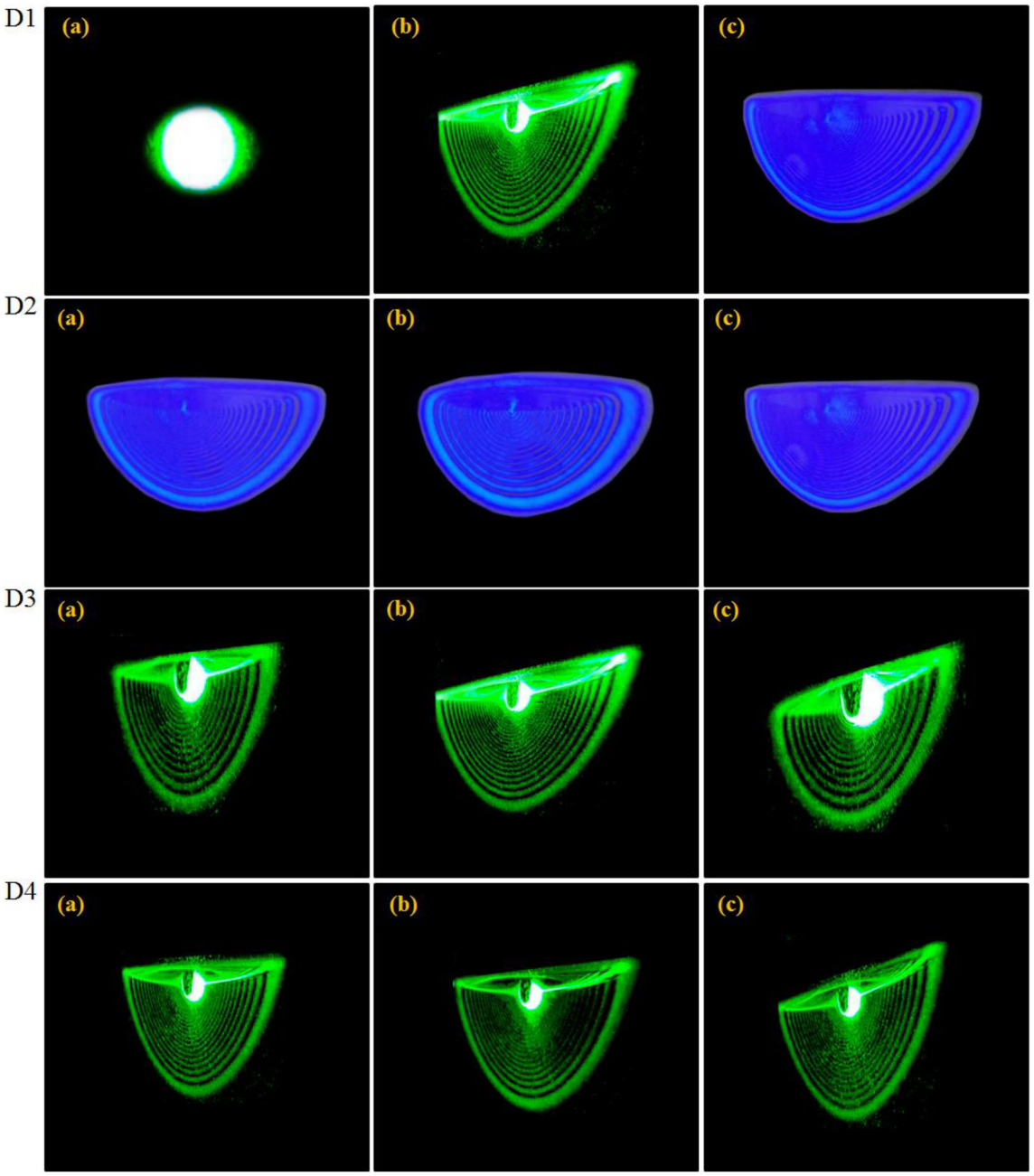

FIGURE 13 D1 (a) Single solid spot with no diffraction rings appeared in the presence of the 532 nm beam only, because the absorption coefficient in Cur-MeO is very low, D1 (b) green patterns appear in the presence of 473 nm, and D1 (c) the blue rings due to the 473 nm beam. D2 (a + b + c) shows the 473 nm beam power effect on the blue rings, D3 (a + b + c) shows the effect of the 473 nm and on the green ring pattern number and area due to the effect of the 473 nm, and D4 (a + b + c) shows the effect of the 532 nm beam on the green intensity only. All these results are in the Cur-MeO.

ANC indicates the occurrence of saturation absorption. In order to obtain a pure INR, Figure 14A data must be divided by Figure 14B data, for each sample, and Figure 14C is the result of the division.

The value of the INR, n_2, and the ANC, β, are given by the following formulas[26]:

$$n_2 = \frac{\Delta\varphi\lambda}{2\pi L_{\text{eff}} I}, \tag{7}$$

$$\beta = \frac{2\sqrt{2}\Delta T}{L_{\text{eff}} I}, \tag{8}$$

$$\text{Where } |\Delta\varphi| = \frac{\Delta T_{p-v}}{0.406(1-S)^{0.25}}, \tag{9}$$

$$\Delta T_{p-v} = T_p - T_v, \tag{10}$$

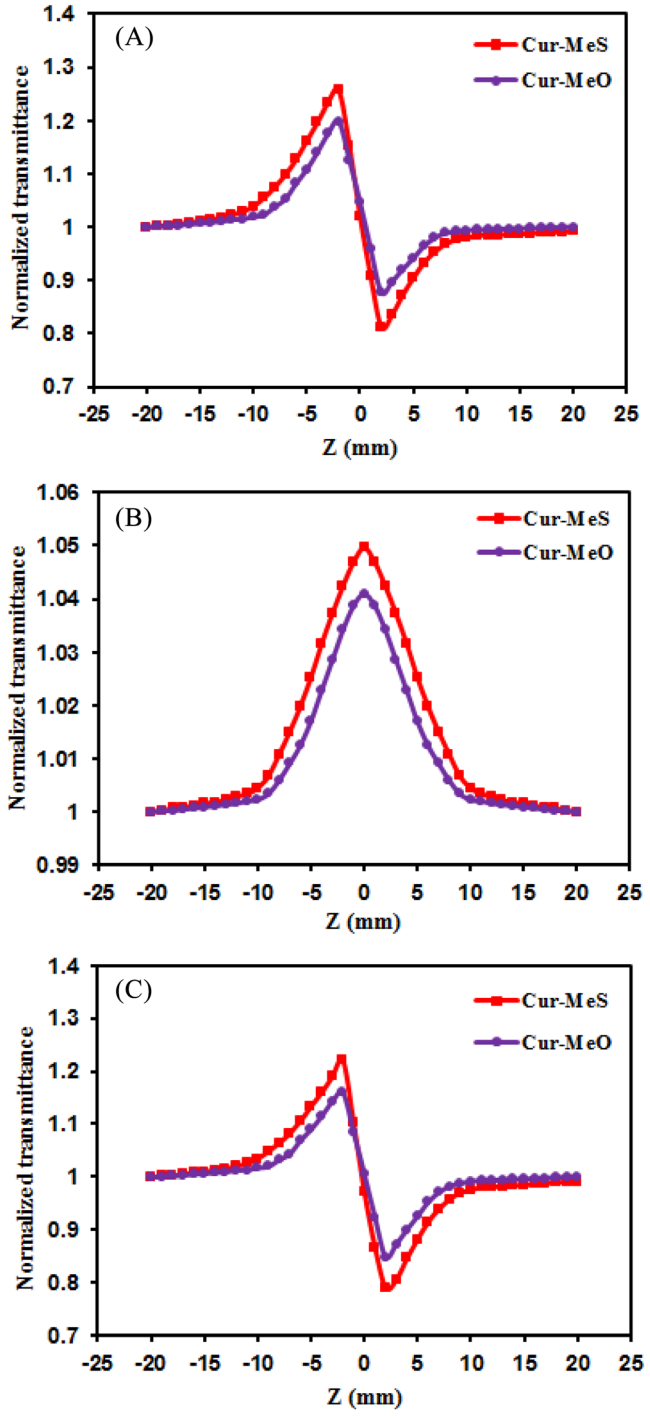

FIGURE 14 (A) Closed aperture (CA) *Z*-scan, (B) open aperture (OA) *Z*-scan, and (C) CA *Z*-scan data divided by OA *Z*-scan data of Cur-MeS and Cur-MeO compounds

$$S = 1 - \exp\left(-\frac{2r_a^2}{\omega_a^2}\right), \tag{11}$$

$$L_{\text{eff}} = [1 - \exp(-\alpha d)]/\alpha, \tag{12}$$

$$\Delta T = 1 - T_p, \tag{13}$$

where ΔT_{p-v} is the transmittance at peak (T_p) minus the transmittance at valley (T_v) in the curve of CA *Z*-scan, S is the linear aperture transmittance, ω_a is the beam radius at the aperture, r_a is the aperture radius, L_{eff} is the sample effective thickness, and ΔT is one minus the transmittance of peak (T_p) in the OA *Z*-scan curve. By finding the ΔT_{p-v} and ΔT values from Figure 14B,C, respectively, and using the input power 5 mW, $I = 860.76\ \text{W/cm}^2$, and Equations 7–13, we find that the values of the INR and the nonlinear absorption coefficient (NAC) for Cur-MeS and Cur-MeO are 2.18×10^{-7} and $1.16 \times 10^{-7}\ \text{cm}^2/\text{W}$ and 3.39×10^{-3} and $2.1 \times 10^{-3}\ \text{cm/W}$, respectively. The variance in n_2 values of both samples using the DRPs and *Z*-scan techniques is due to the power input difference used in both techniques. The n_2 value of the sample Cur-MeS is higher than that of the sample Cur-MeO, which is attributed to the difference between the linear absorption coefficient of the first relative to the second at the wavelength 473 nm, that is, $\alpha_{\text{Cur-MeS}} = 17.02\ \text{cm}^{-1}$ and $\alpha_{\text{Cur-MeO}} = 9.05\ \text{cm}^{-1}$.

4 | CONCLUSION

Curcumin analogues, namely, Cur-MeS and Cur-MeO, were synthesized via the reaction of 3-chloroacetyl acetone and aromatic aldehydes and characterized via FTIR, mass, ^{1}H NMR, and ^{13}C NMR spectroscopies. The nonlinear properties of both samples irradiated with cw visible 473 nm laser beam led to the calculation of the INR and NAC based on the DRPs and *Z*-scans. The INRs of the Cur-MeS compound based on the two techniques were higher than those of the compound Cur-MeO, due to the difference in the linear absorption coefficients of both compounds at 473 nm wavelength. The all-optical switching property using two visible laser beams, namely, 473 and 532 nm, was proved to occur in both Cur-MeS and Cur-MeO samples. Finally, we can confirm that the objective of the current study has been achieved, as two new materials have been found that have high NLO properties.

DATA AVAILABILITY STATEMENT

Data are available in the Supporting Information.

ORCID

Qusay M. A. Hassan https://orcid.org/0000-0002-8941-6816

REFERENCES

[1] G. M. Shabeeb, C. A. Emshary, Q. M. A. Hassan, H. A. Sultan, *Phys. B* **2020**, *578*, 411847.

[2] S. A. Ali, Q. M. A. Hassan, C. A. Emshary, H. A. Sultan, *Phys. Scr.* **2020**, *95*, 095814.
[3] C. A. Emshary, I. M. Ali, Q. M. A. Hassan, H. A. Sultan, *Phys. B* **2021**, *613*, 413014.
[4] H. A. Abdullmajed, H. A. Sultan, R. H. Al-Asadi, Q. M. A. Hassan, A. A. Ali, C. A. Emshary, *Phys. Scr.* **2022**, *97*, 025809.
[5] R. S. Elias, Q. M. A. Hassan, C. A. Emshary, H. A. Sultan, B. A. Saeed, *Spectroch. Acta Part A: Molec. Biomol. Spec.* **2019**, *223*, 117297.
[6] A. M. Jassem, Q. M. A. Hassan, C. A. Emshary, H. A. Sultan, F. A. Almashal, *Phys. Scr.* **2020**, *96*, 025503.
[7] A. M. Dhumad, Q. M. A. Hassan, C. A. Emshary, T. Fahad, N. A. Raheem, H. A. Sultan, *J. Photochem. Photobiol., A* **2021**, *418*, 113429.
[8] Q. M. A. Hassan, N. A. Raheem, C. A. Emshary, A. M. Dhumad, H. A. Sultan, T. Fahad, *Opt. Las. Technol.* **2022**, *148*, 107705.
[9] H. A. Sultan, A. M. Dhumad, Q. M. A. Hassan, T. Fahad, C. A. Emshary, N. A. Raheem, *Spectroch. Acta Part A: Molec. Biomol. Spec.* **2021**, *251*, 119487.
[10] D. Z. Mutlaq, Q. M. A. Hassan, H. A. Sultan, C. A. Emshary, *Opt. Mater.* **2021**, *113*, 110815.
[11] M. F. Al-Mudhaffer, A. Y. Al-Ahmad, Q. M. A. Hassan, C. A. Emshary, *Optik* **2016**, *127*, 1160.
[12] U. J. Al-Hamdani, Q. M. A. Hassan, C. A. Emshary, H. A. Sultan, A. M. Dhumad, A. A. Al-Jaber, *Optik* **2021**, *248*, 168196.
[13] J. Weickert, *Acta Math. Uni. Comenianae* **2008**, *LXX1*, 33.
[14] S. Manickasundaram, P. Kannan, R. Kumaran, R. Velu, P. Ramamurthy, Q. M. A. Hassan, P. K. Palanisamy, S. Senthil, S. S. Narayanan, *J. Mater. Sci. Mater. Electron.* **2011**, *22*, 25.
[15] S. Manickasundaram, P. Kannan, Q. M. A. Hassan, P. K. Palanisamy, *J. Mater. Sci. Mater. Electron.* **2008**, *19*, 1045.
[16] Q. M. A. Hassan, P. K. Palanisamy, S. Manickasundaram, P. Kannan, *Opt. Commun.* **2006**, *267*, 236.
[17] S. Manickasundaram, P. Kannan, Q. M. A. Hassan, P. K. Palanisamy, *Optoelec. Adv. Mat.. Rap. Commun.* **2008**, *2*, 324.
[18] Q. M. A. Hassan, P. K. Palanisamy, *Opt. Las. Tech.* **2007**, *39*, 1262.
[19] F. A. Almashal, M. Q. Mohammed, Q. M. A. Hassan, C. A. Emshary, H. A. Sultan, A. M. Dhumad, *Opt. Mater.* **2020**, *100*, 109703.
[20] Q. M. A. Hassan, C. A. Emshary, H. A. Sultan, *Phys. Scr.* **2021**, *96*, 095503.
[21] K. A. Al-Timimy, Q. M. A. Hassan, H. A. Sultan, C. A. Emshary, *Optik* **2020**, *224*, 165398.
[22] Q. M. A. Hassan, *Mod. Phys. Lett. B* **2014**, *28*, 1450079.
[23] C. A. Emshary, Q. M. A. Hassan, H. Bakr, H. A. Sultan, *Phys. B* **2021**, *622*, 413354.
[24] Q. M. A. Hassan, R. K. H. Manshad, *Opt. Quant. Electron.* **2015**, *47*, 297.
[25] Q. M. A. Hassan, R. K. H. Manshad, *Opt. Mater.* **2019**, *92*, 22.
[26] M. Sheik-Bahae, A. A. Said, T. Wei, D. J. Hagan, E. W. Van Stryland, *IEEE J. Quant. Electron.* **1990**, *26*, 760.
[27] J. W. Daily, M. Yang, S. Park, *J. Med. Food* **2016**, *19*, 717.
[28] I. Chattopadhyay, K. Biswas, U. Bandyopadhyay, R. K. Banerjee, *Curr. Sci.* **2004**, *87*, 44.
[29] A. Rohman, *Int. Food Res. J.* **2012**, *19*, 19.
[30] A. Amalraj, A. Pius, S. Gopi, S. Gopi, *J. Tradit. Complement. Med.* **2017**, *7*, 205.
[31] J. O. Akolade, H. O. Oloyede, A. O. Aliyu, S. A. Akande, A. I. Ganiyu, P. C. Onyenekwe, *Fountain J. Natural Appl. Sci.* **2019**, *8*, 12.
[32] S. V. Jovanovic, S. Steenken, C. W. Boone, M. G. Simic, *J. Am. Chem. Soc.* **1999**, *121*, 9677.
[33] R. Abood, T. Alsalim, E. Abood, *Egypt. J. Chem.* **2021**, *64*, 2173.
[34] Y. Panahi, M. Hosseini, N. Khalili, E. Naimi, M. Majeed, A. Sahebkar, *Clin. Nutr.* **2015**, *34*, 1101.
[35] S. J. Hewlings, D. S. Kalman, *Foods* **2017**, *6*, 92.
[36] E. Ooko, T. Alsalim, B. Saeed, M. E. M. Saeed, O. Kadioglu, H. S. Abbo, S. J. J. Titinchi, T. Efferth, *Toxicol. Appl. Pharmacol.* **2016**, *305*, 216.
[37] V. Basile, E. Ferrari, S. Lazzari, S. Belluti, F. Pignedoli, C. Imbriano, *Biochem. Pharmacol.* **2009**, *78*, 1305.
[38] K. Madden, L. Flowers, R. Salani, I. Horowitz, S. Logan, K. Kowalski, S. Mohammeda, *Cancer Res.* **2008**, *6*, 3940.
[39] R. Prasanna, H. Chandramoorthy, P. Ramaiyapillai, D. Sakthisekaran, *Biomed. Prev. Nutr.* **2011**, *1*, 153.
[40] M. Singh, N. Singh, *Mol. Cell. Biochem.* **2009**, *325*, 107.
[41] P. Khandelwal, A. Alam, A. Choksi, S. Chattopadhyay, P. Poddar, *ACS Omega* **2018**, *3*, 4776.
[42] M. Tomeh, R. Hadianamrei, X. Zhao, *Int. J. Mol. Sci.* **2019**, *20*, 1033.
[43] E. Janiszewska-Turak, A. Pisarska, J. B. Królczyk, *Nauka Przyr. Technol.* **2016**, *10*, 51.
[44] J. Duan, Y. Zhang, S. Han, Y. Chen, B. Lib, M. Liao, W. Chen, X. Deng, J. Zhao, B. Huang, *Int. J. Pharm.* **2010**, *400*, 211.
[45] M. Heger, R. F. van Golen, M. Broekgaarden, M. C. Michel, *Pharmacol. Rev.* **2014**, *66*, 222.
[46] T. M. Kolev, E. A. Velcheva, B. A. Stamboliyska, M. Spiteller, *Inter. J. Quant. Chem.* **2005**, *102*, 1069.
[47] V. Galasso, B. Kovac, A. Modelli, M. F. Ottaviani, F. Pichierri, *J. Phys. Chem. A* **2008**, *112*, 2331.
[48] H. Weiss, J. Reichel, H. Görls, K. Rolf, A. Schneider, M. Micheel, M. Pröhl, M. Gottschaldt, B. Dietzek, W. Weigand, *Beilstein J. Org. Chem.* **2017**, *13*, 2264.
[49] P. Gräb, E. Geidel, *World J Chem Educ* **2019**, *7*, 136.
[50] W. Radhi, B. A. Saeed, *Am. J. Applied Sci.* **2010**, *7*, 1053.
[51] H. Tonnesen, J. Karlsen, A. Mostad, *Acta Chem. Scand.* **1982**, *36B*, 475.
[52] A. Mostad, U. Pedersen, P. Rasmussen, S. Lawesson, *Acta Chem. Scand.* **1983**, *37B*, 901.
[53] A. Mostad, U. Pedersen, P. Bodstrup, S. Lawesson, *Acta Chem. Scand.* **1984**, *38B*, 479.
[54] C. Gorbit, A. Mostad, U. Pedersen, P. Bodstrup, S. Lawesson, *Acta Chem. Scand.* **1986**, *40B*, 420.
[55] C. H. Görbitz, A. Mostad, *Acta Chem. Scand.* **1993**, *47*, 509.
[56] A. Mostad, *Acta Chem. Scand.* **1994**, *48*, 144.
[57] M. A. Addicoat, G. F. Metha, T. W. Kee, *J. Comput. Chem.* **2011**, *32*, 429.
[58] P. Trouillas, P. Marsal, D. Siri, R. Lazzaroni, J. Duroux, *Food Chem.* **2006**, *97*, 679.
[59] T. Alsalim, H. Mzban, E. Abood, *Eur. J. Chem.* **2017**, *8*, 344.
[60] A. Barik, N. K. Goel, K. I. Priyadarsini, H. Mohan, *J. Photosci.* **2004**, *11*, 95.

[61] K. E. Jasim, S. Cassidy, F. Z. Henari, A. A. Dakhel, *J. Eng. Pow. Engin.* **2017**, *11*, 409.
[62] D. Patra, R. El Kurdi, *Gre. Chem. Lett. Rev.* **2021**, *14*, 474.
[63] H. A. Sultan, Q. M. A. Hassan, A. S. Al-Asadi, R. S. Elias, H. Bakr, B. A. Saeed, C. A. Emshary, *Opt. Mater.* **2018**, *85*, 500.
[64] R. S. Elias, Q. M. A. Hassan, H. A. Sultan, A. S. Al-Asadi, B. A. Saeed, C. A. Emshary, *Opt. Las. Technol.* **2018**, *107*, 131.
[65] J. H. Jebur, Q. M. A. Hassan, M. F. Al-Mudhaffer, A. S. Al-Asadi, R. S. Elias, B. A. Saeed, C. A. Emshary, *Phys. Scr.* **2020**, *95*, 045804.
[66] B. A. Saeed, Q. M. A. Hassan, C. A. Emshary, H. A. Sultan, R. S. Elias, *Spectrochim. Acta, Part A: Mol. Biomol. Spectrosc.* **2020**, *240*, 118622.
[67] Y. Jia, Y. Shan, L. Wu, X. Dai, D. Fan, Y. Xiang, *Photosynth. Res.* **2018**, *6*, 1040.
[68] B. L. M. van Baar, J. Rozendal, H. van der Goot, *J. Mass Spectrom.* **1998**, *33*, 319.
[69] S. N. Margar, L. Rhyman, P. Ramasami, N. Sekar, *Spectrochim. Acta, Part A: Mol. Biomol. Spectrosc.* **2016**, *152*, 241.
[70] M. M. Raikwar, L. Rhyman, P. Ramasami, N. Sekar, *Chem Select* **2018**, *3*, 11339.
[71] M. Fontani, A. Colombo, C. Dragonetti, S. Righetto, D. Roberto, D. Marinotto, *Inorganics* **2020**, *8*, 36.
[72] R. Fathima, A. Mujeeb, *Dyes Pigm.* **2021**, *189*, 109256.
[73] F. Z. Henaria, S. Cassidy, *AIP Conf. Proc.* **2015**, *1653*, 020044.
[74] F. Z. Henari, S. Cassidy, K. E. Jasim, A. A. Dakhel, *J. Non. Opt. Phys. Mater.* **2013**, *22*, 1350017.
[75] S. N. Margar, N. Sekar, *Mol. Phys.* **1867**, *2016*, 114.
[76] A. M. Dhumad, Q. M. A. Hassan, T. Fahad, C. A. Emshary, N. A. Raheem, H. A. Sultan, *J. Mol. Struct.* **2021**, *1235*, 130196.
[77] Q. M. A. Hassan, H. Bakr, C. A. Emshary, H. A. Sultan, *Optik* **2020**, *213*, 164771.
[78] Y. Shan, J. Tang, L. Wu, S. Lu, X. Dai, Y. Xiang, *J. Alloys Compd.* **2019**, *771*, 900.
[79] K. Ogusu, Y. Kohtani, H. Shao, *Opt. Rev.* **1996**, *3*, 232.

SUPPORTING INFORMATION

Additional supporting information can be found online in the Supporting Information section at the end of this article.

How to cite this article: A. G. Faisal, Q. M. A. Hassan, T. A. Alsalim, H. A. Sultan, F. S. Kamounah, C. A. Emshary, *J Phys Org Chem* **2022**, e4401. https://doi.org/10.1002/poc.4401